Published in final edited form as:
Neuropathol Appl Neurobiol. 2009 June ; 35(3): 306–328. doi:10.1111/j.1365-2990.2008.01006.x.

Expression of the translocator protein of 18 kDa by microglia, macrophages and astrocytes based on immunohistochemical localization in abnormal human brain

Melissa Cosenza-Nashat[1,2], **Meng-Liang Zhao**[1], **Hyeon-Sook Suh**[1], **Janet Morgan**[3], **Ryan Natividad**[2], **Susan Morgello**[4], and **Sunhee C. Lee**[1]

[1] Department of Pathology, Albert Einstein College of Medicine, Bronx, NY 10461

[2] Department of Science, Borough of Manhattan Community College of the City University of New York, New York, NY

[3] Department of Dermatology, Roswell Park Cancer Institute, Buffalo, NY 14263

[4] Departments of Pathology and Neuroscience, Mount Sinai Medical Center, New York, NY 10029

Abstract

Aims—Microglia are involved in neurodegeneration, are prime targets for anti-inflammatory therapy and are potential biomarkers of disease progression. For example, positron emission tomography (PET) imaging employing radioligands for the mitochondrial translocator protein of 18 kDa (TSPO, formerly known as the peripheral benzodiazepine receptor) is being scrutinized to detect neuroinflammation in various diseases. TSPO is presumably present in activated microglia, but may be present in other neural cells.

Methods—We sought to elucidate the protein expression in normal human CNS, several neurological diseases (HIV encephalitis, Alzheimer's disease, multiple sclerosis and stroke) and SIV encephalitis by performing immunohistochemistry with two anti-TSPO antibodies.

Results—Although the overall parenchymal staining was minimal in normal brain, endothelial and smooth muscle cells, subpial glia, intravascular monocytes and ependymal cells were TSPO positive. In disease states, elevated TSPO was present in parenchymal microglia, macrophages and some hypertrophic astrocytes, but the distribution of TSPO varied depending on the disease, disease stage and proximity to the lesion or relation to infection. Staining with the two antibodies correlated well in white matter, but one antibody also stained cortical neurons. Quantitative analysis demonstrated a significant increase in TSPO in the white matter of HIV encephalitis compared to brains without encephalitis. TSPO expression was also increased in SIV encephalitis.

Conclusions—This report provides the first comprehensive immunohistochemical analysis of the expression of TSPO. The results are useful for informing the usage of PET as an imaging modality and have an impact on the potential use of TSPO as an anti-inflammatory pharmacological target.

Keywords

positron emission tomography; peripheral benzodiazepine receptor; immunohistochemistry; human; HIV encephalitis; Alzheimer's disease; multiple sclerosis

Correspondence to: Melissa Cosenza-Nashat, Dept Science, Borough of Manhattan Community, College of the City University of New York, 199 Chambers Street, N646, New York, NY 10007, mnashat@bmcc.cuny.edu or slee@aecom.yu.edu.

INTRODUCTION

In the central nervous system (CNS), microglia constitute a distinct glial cell population that is derived from haematopoietic cells. As the resident brain macrophages, microglia function as immune sentries, and they become activated in both acute and chronic conditions in a context-dependent manner. While surveillance microglia may help maintain homeostasis in the normal brain effectively, microgliosis may go awry and instigate damage resulting in neurodegeneration and dementia in diseases such as Alzheimer's and HIV-associated dementia (see [1] for review). Although microglia must maintain the balance between neurotoxicity and neuroprotection in injury, the complex network of factors which govern their responses is only beginning to be deciphered [2–5]. It is possible that some components of the network of microglial control can be manipulated for prognostic or therapeutic purposes [6].

The translocator protein 18KDa (TSPO) is a receptor that is part of a multimeric complex including a voltage-dependent anion channel and an adenine nucleotide carrier [7]. TSPO is present in the outer mitochondrial membrane and it plays crucial roles in cell physiology, as evidenced by its sequence conservation from bacteria to humans and that its genetic ablation results in an embryonic lethal [8]. It plays a role in maintaining the mitochondrial membrane potential, but also in cholesterol transport, making it crucial for steroidogenesis [9]. In addition, the TSPO plays roles in cellular proliferation, apoptosis and inflammation as well as porphyrin transport and haem biosynthesis (see [10] and [11] for review). The TSPO is different from the central benzodiazepine receptor in terms of function, structure, expression and pharmacological action [10]. In the CNS, TSPO is thought to be expressed by activated microglia and, in addition, administration of the TSPO ligands in vivo or in vitro results in suppression of microglialactivation including inhibition of cytokine expression [12;13].

Positron emission tomography (PET) is a useful tool to assess neuroinflammation and detection of activated microglia. PET has a unique advantage over other imaging modalities in that real-time cell metabolism and physiologic parameters can be quantified in active disease processes [14]. The best studied TSPO radioligand used in PET imaging has been [^{11}C]-PK11195. Although there have been limitations with this ligand, many have been worked out, and new high affinity ligands have been identified and are being studied [14–16]. PET studies show that there is generally an increased retention of [^{11}C]-PK11195 in various neurodegenerative conditions including HIV encephalitis (HIVE), and its simian model SIV encephalitis (SIVE), Alzheimer's disease (AD), Huntington's disease, multiple sclerosis (MS), Parkinson's disease (PD), stroke, amyotrophic lateral sclerosis, and CNS neoplasms (see [14;15] for review). Traditional autoradiography studies of postmortem tissues confirm that TSPO binding sites are increased in many of these diseases and that these binding sites are primarily in microglia. Use of TSPO-binding radioligands to assess neuroinflammation via PET imaging indicates that they may have value as a biosensor of ongoing disease and may also be a target to reduce inflammation-mediated damage in diseases such as HIV-associated neurological disorders and dementia ([17] and see [15;18] for review).

Analysis of the TSPO expression in CNS remains of interest for several reasons. In the laboratory, autoradiography has chiefly been used for visualizing the actual binding sites of the TSPO ligands. Unfortunately, because of its well-known disadvantages including limited resolving power, its use of radioactivity and a processing time in the week-to-month range, autoradiography remains a very limited tool. Immunohistochemical determination of TSPO expression in the human CNS would be an adjunctive means of studying TSPO [14]. Mapping the cellular localization and the degree of expression of TSPO by immunohistochemistry (IHC) will better inform our usage and understanding of PET as an

imaging modality. An increased understanding of TSPO cellular expression is also important because it is being considered as a prognostic marker in types of non-CNS cancers [19–21] and may prove useful for gliomas as well. Additionally, since TSPO ligands have anti-inflammatory properties, suggesting a role for TSPO in neuroinflammation [12;13;22], an understanding of its cell type expression in various disease states may be a key resource in how to target the TSPO in these diseases. In the current study, IHC with two different antibodies against TSPO was utilized to determine the cell-type specific expression and the distribution of the receptor in the human CNS, with emphasis on HIVE and AD. The results demonstrate that a variety of CNS cells are capable of expressing TSPO but that the pattern of expression differs between normal and diseased CNS, as well as among different diseases and cell types. However, microglia and macrophages remain the chief cell type upregulating the TSPO expression in diseased brains.

METHODS

Patient Material

Formalin-fixed, paraffin-embedded brain tissue from cases from the Manhattan HIV-1 Brain Bank of the National NeuroAIDS Tissue Consortium (NNTC) were grouped based on HIV-serostatus and the presence of brain infection: HIV-seronegative (HIV−, n=4)), HIV-seropositive without encephalitis (HIV+, n=5) and HIVE (n=10). The majority of sections contained cerebral cortex (frontal, temporal or parietal) and associated white matter, but some were derived from only cerebral periventricular white matter and others from basal ganglia (see Tables 1 and 3 for details). HIVE sections for study were chosen based on the presence of multinucleated giant cells and microglial nodules on H&E and/or presence of HIVgag p24 expression by IHC. The details with regards to age and sex for all but one of the cases from the NNTC have been previously reported [23;24]. The additional section (Case 38) was from a 47-year old black female.

In addition to standard tissue sections, tissue microarray (TMA) slides prepared by the Manhattan HIV Brain Bank were also utilized for this study. TMA consisted of a composite of six cases (two each of HIV−, HIV+ and HIVE), each represented in two 1-mm tissue punches on a single slide. TMA ensured that the different brain tissues were subjected to identical staining conditions thus eliminating variables (S. Morgello et al., manuscript in preparation).

While HIVE was a primary focus of this study, we have also studied postmortem human brains with several other diseases in which previous studies have indicated upregulation of TSPO. These included Alzheimer's disease (AD), multiple sclerosis (MS) and ischemic infarcts. All AD cases (n=9, courtesy of Dr. Peter Davies) were derived from the hippocampus and adjacent temporal cortex and white matter. Three AD cases were available as free floating vibratome sections and the other six were standard formalin-fixed, paraffin-embedded sections. Brain sections with MS plaques or ischemic infarcts were derived from the Albert Einstein College of Medicine Neuropathology Archives. Brain regions with lesions were selected for IHC based on histological analysis of H&E sections. These included sections from the occipital periventricular white matter (chronic silent MS), pons (acute MS), basal ganglia (chronic infarct) and cerebellum (subacute and old infarcts). The numbers of cases and origin of the sections is indicated in Table 1. The use of human material has been approved by the Institutional Review Boards of both the Borough of Manhattan Community College and the Albert Einstein College of Medicine.

Animal specimens

Paraffin-embedded tissue sections from macaques (courtesy of Dr. Clayton Wiley) were also studied for TSPO expression. One specimen was derived from an uninfected rhesus monkey (SIV−), while three were from SIV-infected macaques, two (one pigtailed and one rhesus) with encephalitis (SIVE) and one without encephalitis (SIV+, rhesus). All sections were derived from anterior basal ganglia (caudate and putamen) with adjacent cerebral cortex and associated white matter. The animals were housed at the University of Pittsburgh in accordance with the American Association of Laboratory Animal Care and the Institutional Animal Care and Use Committee of the University. The strain used to infect the three SIV-infected macaques was a SIVDeltaB670viral swarm. Detailed information regarding the animal protocols has been published previously [25].

Single-label colorimetric IHC for the TSPO

Deparaffinized brain sections were boiled for antigen retrieval in sodium citrate buffer (DAKO, Carpinteria, CA), treated with 3% H_2O_2, blocked with normal goat serum, and then incubated with the primary antibody over night at 4°C, as described [23;26]. Staining for TSPO was completed using two different antibodies: a rabbit polyclonal antibody generated against a C-terminal synthetic fragment based on the known human TSPO sequence [27] and a mouse monoclonal antibody generated against a nearly identical c-terminal sequence of human TSPO [28]. While both antibodies were generated against a similar C-terminal fragment, the peptide was linked to a different immunogenic carrier. The mAb has a tyrosine at the amino end and was linked to albumin, while the pAb was linked to keyhole limpet haemocyanin via a cysteine. For the rabbit polyclonal antibody, IHC was performed as described [27] using the LSAB2 kit (DAKO), which contains reagents for an avidin biotin complex method. As a negative control, sections were incubated with normal rabbit serum. For the mouse monoclonal antibody, the ImmPRESS anti-mouse Ig peroxidase kit (Vector Laboratories, Ltd., Burlingame, CA) was used according to the manufacturer's instructions. Diaminobenzidine (DAB, brown) was utilized as the chromogen for TSPO, sections were dehydrated and mounted. All washes in between steps were completed with phosphate buffered saline (PBS). Single labeled sections were counterstained with hematoxylin after the chromogen step. For a summary of all antibodies, their sources and the method of staining used see Table 2.

Double-label IHC for the TSPO and Cellular Markers

Double label colorimetric IHC was performed for the TSPO along with cell-specific markers, HIV-1 antigen or amyloid-β 40 (Aβ). For cell markers that are monoclonal (CD45RB, CD68 and HIV-1 p24), the rabbit anti-TSPO was used for the double label IHC. For polyclonal antibodies anti-GFAP and anti-Iba1, and monoclonal anti-Aβ, the mouse monoclonal anti-TSPO antibody was used. The TSPO staining was completed as above, but the sections were placed directly into the second primary antibody for the cell marker after the chromogen step. Immunostaining for colorimetric IHC was performed sequentially such that the first antibody was developed with DAB (brown), followed by the second primary antibody and then the alkaline phosphatase-labeled secondary and 5-bromo-4-chloro-3-indolyl phosphate with nitro blue tetrazolium (blue). For AD cases, after the TSPO stain was complete, sections were treated with 90% formic acid for 15 minutes and washed with 1 M Tris solution before the anti-Aβ antibody was applied. After all steps were completed, for all double labeling experiments, sections were not counterstained, but were dehydrated and mounted. See Table 2 for the antibody concentrations and methods used.

Fluorescent double label IHC for TSPO and cellular markers was also performed similar to the colorimetric staining. Immunostaining for fluorescent IHC was performed sequentially such that staining with TSPO was completed first with fluorescein (green), followed by the

second primary and an Alexa fluorophor125 594-conjugated (red) secondary antibody. After the last step was completed, slides were not dehydrated, but were counterstained with DAPI and were mounted using Vectashield Mounting Medium (Vector Laboratories, Ltd.) to limit background auto-fluorescence of the tissue. See Table 2 for the antibody concentrations and methods used.

Antibody Absorption for the Rabbit Polyclonal anti-TSPO Antibody

Two sections were subjected to IHC side by side as described above, but one received the primary antibody that was pre-incubated with a 20-fold excess of recombinant mouse peripheral benzodiazepine receptor protein (Trevigen, Gaithersburg, MD) for two hours prior to the primary antibody incubation step. The remainder of the steps for single-IHC for the TSPO remained the same.

Digital image capture

Bright field images were captured using a Leica Leitz DMRB microscope with an Olympus DP12 digital camera. Fluorescent images were captured with an Olympus IX81 electronically motorized microscope fitted with a Sensicam QE cooled CCD camera, which was connected to a computer.

Quantitative analysis of TSPO staining and image analysis

Nineteen cases from the Manhattan HIV-1 Brain Bank and four macaque brains from the University of Pittsburgh were single stained, most with both antibodies and most as serial sections. The TSPO staining in single-stained slides was first analyzed semi-quantitatively by two independent observers using a grading system from no staining (−) to high levels of intense staining across the slide (++++) in various cell types, with good agreement between the two observers. Cell types were assessed morphologically. Microglia and macrophages were graded up to ++++. Immunoreactive astrocytes, neurons, and vessels were analyzed using the scale similar to microglia/macrophages, except that the highest levels of staining were only ++.

In addition to semi-quantitative analysis, quantitative analysis was performed. After images were captured, the amount of staining was quantitatively analyzed using NIH ImageJ, a downloadable public domain Java-based image processing program [29]. Cases of conditions other than HIV were not analyzed because corresponding normal controls were not available from each site.

Twenty random 400X images per stained section were captured from the white matter regions of the brain. White matter regions were selected for their density of glial cells and because the majority of the sections available were primarily composed of white matter. Since images were stained with DAB (brown) and counterstained with haematoxylin, the images were prepared using ImageJ such that the blue colour was removed and the brown staining remaining was assessed according to previously published methods for multicolored images [30]. A single threshold for background staining was used to process the images. The entire image was used for analysis except in rare instances where intravascular staining or staining artifact was present, in which case these items were removed with the marquee tool. The amount of staining is expressed as the percent area fraction of pixels of the desired colour (in this case, brown for DAB) which indicates the proportion of the image area that is stained. The data for the three groups was compiled for statistics and is presented as the average percent area stained for all cases of a single test group. The HIVE cases with concurrent infections (one had neurosyphillis and had CNS lymphoma) were not used for image analysis.

To assess the propensity of vascular staining, the number of microscope fields with TSPO-labeled endothelial or smooth muscle cells were counted as a percentage of total fields analyzed for each case (HIV−, n = 4; HIV+, n = 4; and HIVE, n = 5). Twenty 400X fields were analyzed per case.

Statistical analyses

Statistics were performed using GraphPad Prism Version 4.0. For the overall image analysis of white matter and the vascular staining analysis, data among the three groups (HIV−, HIV + and HIVE) were compared for each antibody. Kruskal-Wallis analysis of variance was performed to compare among groups, while Dunn's multiple comparison tests were carried out for pairwise comparisons. In order to compare the staining capabilities of the two antibodies, Spearman correlation analysis was performed for cases in which serial sections were available.

RESULTS

TSPO expression in normal human brain

Two antibodies, a mouse monoclonal (mAb) and a rabbit polyclonal (pAb), were used to immunolabel the brain sections. Cell staining was present in both the gray matter (Figure 1A and B) and the white matter (G, H)(also see Table 3). The quality of the staining was punctate which is consistent with the reported mitochondrial localization of TSPO protein. Due to the punctate nature of the cell processes, often complete cell shapes could not be deciphered. Occasionally, positively stained process-bearing cells were identifiable as glial cells (C, D, E), resembling microglia or astrocytes. Rarely, TSPO+ cells resembling oligodendrocytes were also observed (not shown, but see Figure 2 for macaque brains). No staining was observed with the control rabbit serum or normal mouse IgG1 (not shown). The pAb (but not mAb) labeled neuronal cell bodies with punctuate spots (B), and both pAb and mAb labeled some endothelial cells (F) and smooth muscle cells, in agreement with other studies [27;31]. The vascular endothelial and smooth muscle cell stain were also highly punctate. In general, the mAb was better than the pAb in staining vessel-associated TSPO. Additional cells/areas in which TSPO immunoreactivity was observed in normal brains as well as diseased brains included subpial glia (both astrocytes and microglia, Figure 1C), meninges (vessels, macrophages, and sometimes arachnoid cells; not shown), ependymal cells, subependymal glia (both astrocytes and microglia), choroid plexus (vessels, macrophages, and choroid plexus epithelial cells, not shown), as well as intravascular monocytes (not shown). Again, the staining pattern in these cells tends to be punctate or granular.

Expression of the TSPO in HIV+ and HIVE

The HIV+ brains (Figure 1I and J) showed a range of staining (none to delicate) similar to that in normal brain (see also Table 3). Two cases showed virtually no staining other than vessels, while two other cases showed gray matter staining of delicate processes. Some of the positive cells resembled "metabolic glia," a form of reactive astrocytes with large swollen nuclei, while others resembled microglia (not shown). The white matter stain in some HIV+ cases (Figure 1I and J, for example) from the tissue microarray demonstrated delicate, punctate process staining, reminiscent of microglia.

The HIVE brains displayed staining in compartments observed in normal cases (such as meninges, ependymal cells and subependymal glia—both astrocytes and microglia—and intravascular monocytes), but also showed markedly enhanced staining in the parenchyma, particularly in regions of infection. In cases where the infection was diffuse [23], ramified glial cells had enhanced TSPO positivity, most of which were clearly identifiable as

activated microglia. All cases also showed TSPO+ perivascular macrophages. At low power, the TSPO+ areas were identifiable as microglial nodules and multinucleated giant cells (MGCs) (Figure 2A, B). TSPO+ hypertrophic astrocytes were also present in HIVE cases based on morphology (Figure 2A–C, also see Table 3). The subcellular distribution of TSPO in reactive astrocytes appeared more diffusely cytosolic, especially with the pAb. In addition, superimposed discrete punctate staining was present in most TSPO+ astrocytes. These puncta were often (but not always) arranged in the periphery of the cell body. Microglial staining was also present in the gray matter, especially in areas of HIV infection where staining was prominent (not shown). Infiltrating T lymphocytes present in many of these brains [32], appear negative for TSPO. Of note, a CNS lymphoma in HIVE demonstrated tumour cells to be TSPO+, as well as the infiltrating macrophages and phagocytic microglia (not shown). Oligodendrocyte staining was not readily evident in the HIVE brains. Semi-quantitative analysis of cell type expression based on TSPO+ cell morphology was performed for the single-stained sections of HIV−, HIV+ and HIVE (Table 3).

Expression of TSPO in macaque brains

Two SIVE and one each of SIV+ and SIV− brains were examined for TSPO expression. All sections came from the same region of the brain, at the level of anterior basal ganglia and adjacent cortex. Cell types observed to be TSPO+ in normal human brain, such as meningeal cells, ependymal cells, subependymal glial cells, endothelial cells and vascular smooth muscle cells, were also TSPO+ in macaque brains. In addition, the choroid plexus was also immunoreactive, in agreement with rodent autoradiography studies [33;34]. Curiously, neurons were much less often TSPO+ with the pAb in simian brains. The very few TSPO+ neurons showed intense granular staining (not shown). Similar to human brains, all macaque brains displayed both TSPO+ ventricular and meningeal surfaces, though subpial and subependymal gliosis was much milder (not shown). In macaque brain, the parenchymal glial process staining was sparse and delicate in SIV− and SIV+ brains, while in SIVE brains, this was greatly enhanced. The two SIVE cases had very different types of pathologies, one characterized by a dense perivascular mononuclear infiltrate without MGC, and the other by numerous MGCs in the perivascular and subarachnoid spaces (with associated macrophages and lymphocytes). Microglial nodules were rare. In the former, the TSPO immunoreactivity was shown as striking diffuse reactive microgliosis (Figure 2F) in both the gray and white matter. The TSPO immunoreactivity in the latter was present primarily in MGCs and macrophages (Figure 2G–J), but rarely in microglia. An additional point of interest was that TSPO+ oligodendrocytes were present in the optic tract (and vicinity) in one SIVE and the SIV− brain (Figure 2E). What were noticeably lacking in SIVE were the TSPO+ hypertrophic astrocytes that were present in most HIVE cases. Semi-quantitative analysis of TSPO+ cell type expression in macaque brains is summarized in Table 3.

Qualitative comparison of two TSPO antibodies

Many sections used in this study were examined by both of the antibodies (see Table 3) so that direct comparisons could be made. For example, all HIV−, HIV+ cases as well as selected HIVE cases were studied by both. In addition, all macaque brains were also stained with both. The most striking difference is the presence of neuronal staining only with pAb. The second is the prominence of vascular staining with the mAb more than with pAb. In addition, in case of diffuse microgliosis, the mAb appear to stain them better than the pAb. The third is that mAb was better in detecting TSPO+ hypertrophic astrocytes.

Nevertheless, in tissue microarray preparations (see Methods), the two antibodies showed good correspondence. The images in Figure 1 panels G–L were taken from two serially

sectioned tissue microarray slides on which six cases were represented as duplicate 1-mm tissue punches. Despite some qualitative differences previous mentioned, the images of staining of serial sections in G–L indicate that the two antibodies have a good agreement overall with the quality and the levels of staining in the white matter. Detailed quantitative analysis of TSPO staining for these groups is presented below.

Antibody absorption for the pAb

The neuronal staining observed with the pAb (Figure 1B) was intriguing since TSPO ligand binding has not been reported in human neurons, although it was reported in some types of rodent neurons [35;36]. To determine the specificity of neuronal (and other cell) staining with the pAb, we performed a protein absorption study. When the TSPO protein was incubated with the primary antibody, the glial cell staining was reduced to approximately half (52% by ImageJ) but the neuronal staining was not reduced (not shown). The experiment was not repeated because the cost of the peptide was prohibitive, but the results might imply that the neuronal staining is non-specific (see Discussion).

Quantitative immunohistochemical analysis for HIVE

An analysis comparing TSPO+ immunoreactivity in HIV−, HIV+ and HIVE brains was only performed with the tissue from the NNTC since a complete set of normal controls was available from the same source. While tissue microarray was useful for comparisons, it limited the number of images that could be captured of each case for analysis. We therefore proceeded to stain multiple HIV−, HIV+ and HIVE sections. Since white matter has been shown to be important in TSPO ligand binding in SIVE [37] and the majority of the sections studied had a propensity of white matter, we focused our analysis on the white matter expression of TSPO.

Image analysis of TSPO-stained brain sections was performed using NIH ImageJ. Twenty random 400X microscope fields of white matter per case were analyzed for each antibody. Staining is expressed as the percent area stained and is displayed in a box and whisker diagram (Figure 3A). The staining in HIV− cases ranged from 0.02–0.12% area stained for the mAb and 0.03–0.11% for the pAb. The percent area stained in the HIV+ group ranged from 0.01 to 0.10% for the mAb and 0.01 to 0.08% for the pAb. In HIVE, TSPO levels ranged greatly such that some areas appeared to have low, normal-appearing TSPO expression while microglial nodules had very high levels of TSPO. The average percent area stained for HIVE cases ranged from 0.27 to 1.24% for the mAb and 0.01 to 0.5% for the pAb. Some nodules had very high TSPO labeling; the highest observed TSPO expression in the captured images was 4.7% area stained (which contributed to the large range shown for the HIVE cases). The percent area stained among the groups (HIV−, HIV+ and HIVE) was analyzed by Kruskal-Wallis analysis of variance and it was found to be significantly different for both antibodies ($p < 0.001$). Analysis of the average immunolabeling between groups indicated that the percent area stained for both the HIV− group and HIV+ group were significantly different from the percent area stained of the HIVE group (based on Dunn's multiple comparison test, $p < 0.001$ for pair-wise comparisons marked by *) for both antibodies. The percent area stained between HIV− and HIV+ groups was not significantly different for either antibody.

For a number of cases ($n = 8$), serial sections from the same block were available to test whether the staining for both antibodies in the same block of the same case was correlated. The Spearman correlation analysis denoted that the relationship between percent area stained by both antibodies is correlated ($p < 0.05$; Spearman $r = 0.08$). The linear relationship between the percent area stained by the pAb and the mAb is shown in Figure 3B.

In addition to glial cell staining, vascular staining was also quantified in HIV− (n=4), HIV+ (n=4) and HIVE (n=5) cases by calculating the percentage of 400X fields (twenty analyzed per case) exhibiting TSPO labeling of endothelial and smooth muscle cells. Because of the superior ability of the mAb to stain vasculature, only the sections stained with the mAb were analyzed in this manner. The results show that TSPO+ vessels appeared in approximately one out of three 400X fields on average, with no differences observed between the groups (Figure 3C). These results suggest that in contrast to glial staining, endothelial TSPO staining may be constitutive. Qualitatively, however, the staining intensity in some HIVE cases appears to be higher (not shown).

Double label IHC identifies microglia, macrophages and astrocytes to be TSPO+

To confirm TSPO+ glial cell identity, double IHC was employed in HIVE brains. CD68, a macrophage-lineage marker was first used to identify TSPO+ macrophages and microglia and this showed many double-positive cells, many of which are process-bearing (Figure 4A, D). Most MGCs were CD68+ and TSPO+ (Figure 4B). The leukocyte marker CD45 also demonstrated double-positive perivascular macrophages as well as MGCs (Figure 4E, F). In regions of active HIV replication, as indicated by HIV-1 p24 immunolabeling (Figure 4C, G), most HIV-infected cells were also TSPO+ (arrowheads). These results confirm that macrophages and microglia are the major TSPO+ cell populations in HIVE.

Double labeling with the astrocyte marker GFAP showed that astrocytes can express TSPO (arrowheads, Figure 5A, D), but that astrocyte expression was not as widespread as microglial expression. In some cases, the area of TSPO+ astrocytes coincided with a region of active HIV replication, based on HIV-1 p24 staining (Figure 5B). TSPO+ microglia (GFAP−, arrows in all panels) were much more abundant than TSPO+ astrocytes (Figures 5C and E).

Expression of TSPO in MS

Several different types of MS lesions were stained for TSPO using the pAb. The same chronic silent demyelinated plaque is shown with H&E and TSPO labeling (Figure 6A and B, respectively). The demyelinated region is indicated with arrowheads in A. TSPO stain is present in scattered fibrillary astrocytes (arrows, B; high power in C). Note that adjacent normal-appearing white matter is devoid of staining. In another brain, an acute MS lesion is shown to contain a number of phagocytic macrophages throughout the plaque, which were also TSPO+ (Figure 6D). Adjacent brain showed neuronal staining as well as focal microglial staining. These results suggest that macrophages and microglia represent the bulk of TSPO+ cells in acute MS but that in chronic silent MS lesions, reactive astrocytes can also express TSPO.

Expression of TSPO in ischaemic infarcts

Several different stages of infarcts were examined for TSPO with the pAb. In a sub-acute infarct in the cerebellar cortex, scattered amoeboid microglial cells, many of those surrounding Purkinje cells, were TSPO+ (arrowheads, Figure 6E). In a large cystic (old) infarct in the basal ganglia, the phagocytes filling the cystic space were strongly TSPO+ (Figure 6F & G). In addition, the brain areas adjacent to the infarct showed many positive hypertrophic TSPO+ astrocytes, as well as amoeboid microglia with punctate TSPO+ stain (Figure 6F & G). The sections from brains with ischaemia were large and TSPO expression was limited to the lesion and areas juxtaposed to the lesion, but areas away from the lesion exhibited reduced, normal levels of TSPO (not shown).

Expression of TSPO in AD

Sections of the hippocampus and adjacent temporal cortex and white matter from nine AD cases were examined for TSPO expression. All cases were stained with the pAb and some were stained with the mAb. The mAb (no neuronal staining) gave a distinct advantage in viewing AD pathology. In AD, TSPO+ glial cells were widespread in the hippocampus and adjacent brain regions of all cases. This included all sectors of Ammon's horn and dentate gyrus, including the molecular layers and the adjacent white matter (Figure 7A and B). The numbers of positive glial cells varied depending on the case. The temporal neocortex also showed widely dispersed TSPO+ glial cells (Figure 7A). The majority of TSPO-expressing parenchymal cells in AD were microglia as shown with a macrophage marker, Iba1 (Figure 7C, E), but TSPO+ ($Iba1^{-}$) astrocytes were also evident by morphology or by double labeling with GFAP (arrowheads in C, E and not shown). Clusters of TSPO+ cells were also localized within or surrounding senile plaques, as observed with a stain for β-amyloid (Figure 7D, F). β-amyloid was also detected in vessels which were TSPO+ (Figure 7G).

DISCUSSION

The current study is a comprehensive analysis of TSPO immunoreactivity with two different anti-TSPO antibodies in normal and diseased human brain. IHC with three different commercial antibodies, one in our hands and two by a colleague (S. Venneti, personal communication), had been attempted before success was achieved with the two laboratory-derived antibodies used in this study. These antibodies have been previously used to stain skin [27;38], various other peripheral tissues [28], an assortment of tumours including CNS neoplasms, and neuropathological conditions such as AD, MS and PD [31;39;40]. We find that these antibodies were both useful and generally had good agreement in their level of staining (see Figure 1 and Table 3), although there were some differences. It is important to note that while the antibodies were generated with a similar C-terminal fragment, their epitopes might be distinct, which would account for some of their differences in detecting TSPO expression. In addition to the different animal species from which the antibodies were derived and the slightly different methods utilized to produce these antibodies, the differences between the cell-specific staining of the two antibodies (Table 3) may also have been, in part, due to the sensitive micropolymer-based secondary antibody method (ImmPRESS) adopted for the mAb. Nevertheless, the two antibodies had good correspondence with regard to microglial, macrophage and astrocyte staining. The present study can be used in conjunction with autoradiography data, but the results should be interpreted independently since the binding sites of radioligands and histochemical antibodies may be different. One study in an animal model of neurotoxicity found a discrepancy between ligand binding and immunohistochemistry [33], and others have noted that this is perhaps due to the differential binding sites of antibodies and radioligands such as PK11195 [41].

Our study is the first demonstration of TSPO IHC in HIVE and stroke and the first comprehensive study of cell type expression in AD, although previous studies have reported TSPO protein expression [31;39;42;43]. In regards to normal brain, our results complement those from autoradiographic studies [33;43] and confirm that TSPO expression is minimal. TSPO expression in ependymal cells and choroid plexus has also previously been noted [15]. In addition, we confirm that microglia and macrophages are the predominant cell type expressing TSPO in diseased brains and that astrocytes can also express TSPO in humans. Upregulation of TSPO has been confirmed by IHC only recently for gliomas and in AD [31;42;43]. Tomasi et al. performed anti-TSPO IHC along with autoradiography in AD [31]. Although they emphasized vascular immunoreactivity, glial TSPO staining was also apparent (see Figure 7 in [31]). Others have reported that increased TSPO may be present in the frontal cortex of AD brains in both microglia and astrocytes based on autoradiography

for TSPO and assessment of gliosis [44]. Takaya et al. also reported TSPO+ microglia in MS and PD brains, although cell-type specific analysis was not performed [39]. It is generally accepted that microglia and macrophages are the primary cell types exhibiting an increased number of TSPO binding sites in human pathologies, and that astrocytes are not significant contributors to increased TSPO binding sites [44;45].

Previous studies using autoradiography and co-localization of cellular markers with IHC have been performed in various human CNS diseases and in animal models of these diseases (see [14;18] for review). Based on traditional autoradiography and IHC for cellular markers, in peripheral tissues, TSPO has been shown to be present in epithelial cells (exocrine and endocrine), endothelial cells, immune cells such as macrophage-lineage cells and hepatocytes [27;28]. In the human CNS, microglia and endothelial cells have been shown to express TSPO readily ([31] and see [14] for review). Our study confirms this and indicates that microglia strongly express TSPO in the cell body and in processes (Figures 1,2), where mitochondria would be located. While most studies agree that TSPO upregulation occurs in disease-associated microglia, elevated microglial TSPO is not always observed. For instance, tumour-infiltrating microglia in anaplastic astrocytomas were apparently devoid of TSPO immunoreactivity and it was speculated that tumour cells might actively suppress microglial TSPO [39]. That may not be the case for all tumours, however, because we observed phagocytic microglia throughout a CNS lymphoma in one HIVE case (not shown). Differing mechanisms are likely occurring in various tumour types.

In contrast to microglia, astrocytic TSPO has been observed in various conditions in rodents [33;46;47], but TSPO+ astrocytes have been rarely observed in humans and are particularly noted in hepatic encephalopathy [48]. Venneti et al. observed that microglia are the major cells contributing to increased radioligand binding in AD brains, but that astrocytes are not a negligible factor [44]. In the current study, the subcellular distribution of TSPO in human astrocytes is both diffuse and punctuate. Others have shown that TSPO can be present in non-mitochondrial locations that may account for this observation [15;33;49].

Studies that observed TSPO upregulation in both astrocytes and microglia suggest that their expression is temporally distinct [33;46;47]. Using various rodent models of neurotoxicity and demyelination, Guilarte and colleagues speculated that microglial TSPO is upregulated soon after damage and is resolved quickly, but that the onset of astrocytic expression is delayed but it is then persistent [33;47]. This is different from the work done by Chen et al., who observed that the opposite was the case and that microglial binding sites persisted in the rat model of ethanol-induced neurotoxicity, while the astrocytic response was transient [46]. In our study, TSPO+ astrocytes were present in all human disease states, but much less frequently than TSPO+ microglia, suggesting that astrocytic expression may be shorter-lived and/or it occurs only in a subset of astrocytes. Astrocytic expression also tended to be observed in chronic conditions (such as HIVE, chronic MS plaques and AD). The lack of astrocytic staining in SIVE is interesting in light of the studies demonstrating microglia and not astrocytes having increased TSPO ligand binding in SIVE [37;50]. It is possible that TSPO+ astrocytes were not observed in SIVE because of the limited number of cases studied (two), the shorter disease span in monkeys compared with humans, or because there is a true species difference (albeit that seems unlikely).

Based on previous work with activation markers and the reported PET studies employing the TSPO radioligands, we anticipated that microglial TSPO would be elevated in HIVE and SIVE. We also anticipated there to be a slight increase in TSPO positivity in HIV+ (and SIV +) cases, since our work with several immune markers indicated microglial activation in some HIV+ individuals [23]. It is unclear whether the lack of TSPO upregulation in HIV+ cases represents lack of observable microglial activation in these particular cases or regions

studied, or whether HIV infection is required for TSPO upregulation. We feel the latter is unlikely considering that TSPO expression is present in various disease states. Nonetheless, our results are consistent with those by Venneti et al. which showed no significant increase in TSPO radioligand binding in HIV+ individuals [51]. Wiley et al. observed that HIV+ cognitively impaired individuals (post-HAART) did not show an increase in TSPO radioligand binding [51]; however, in both SIVE and HIVE, increased binding of TSPO radioligands were readily demonstrable [52;53]. Although these studies are not analogous to each other (clinical versus pathologic entities), this may be evidence that viral replication is playing a role in TSPO upregulation in HIV/SIV-infected brain.

Endothelial and smooth muscle cell staining for TSPO in vasculature has been observed [27;31]. In AD, Tomasi et al. showed that the presence of TSPO staining in vessels decreased with age and in the presence of AD [31]. We observed that TSPO+ vasculature was present in brains regardless of whether they were HIV−, HIV+ or HIVE and there does not seem to be a significant increase in HIVE brains, suggesting that unlike glial cell TSPO, endothelial TSPO might be constitutive. This observation is important because cerebrovascular expression of TSPO would impact the binding and distribution of TSPO ligands in the brain parenchyma. Since endothelial expression is present in normal CNS, this may indicate a functional compartment of TSPO separate from the glial compartment, which is regulated differently in a disease-dependent manner.

The neuronal staining observed with the polyclonal antibody remains a conundrum. The specificity of both antibodies has been confirmed by immunoblotting and subcellular localization has been verified by electron microscopy [27;28;54]. Neuronal expression of TSPO has been observed in rodents [35;36;55] but not in humans and we originally believed the staining to be non-specific. Our antibody absorption experiment supports this notion; however, we cannot dismiss neuronal TSPO as non-specific based on the following reasons. First, it is possible that the antibody absorption was not 100% effective because the protein used was derived from the mouse. Second, the distribution of TSPO in neuronal cell bodies was punctate, suggestive of mitochondrial distribution. Third, studies have shown that different human (and other mammalian) isoforms of TSPO exist [56–58]. Thus, it is possible that the neuronal form represents a different isoform or a structurally related molecule which is not yet identified. In light of these findings, it is of interest to speculate whether some of the gray matter TSPO radioligand binding (compared to white matter) observed in some PET studies ([37;59;60] and see [14] for review) is due to neuronal binding. Variable TSPO isoforms may also explain different affinities of ligands [16] for the TSPO and would have ramifications for the potential use of ligands as therapeutics.

The mechanisms regulating TSPO expression in microglia and astrocytes are unknown. Papadopoulos and colleagues have shown that the Sp1/Sp3 and members of the Ets family of transcription factors control basal expression of the TSPO [61]. Less is known about the transcriptional elements involved in the inducible expression of this molecule; however, inflammatory cytokines such as interleukin-1β, tumour necrosis factor-α and interferon-γ have been shown to increase levels of TSPO in various cell types, including astrocytes [62–65], indicating the presence of cellular mechanisms that upregulate TSPO during inflammation. Our own preliminary data indicates that interleukin-1β can increase TSPO in primary human astrocytes (not shown). The purported involvement of TSPO in neuroinflammation and neurological disorders (see [18] and [66] for review) points to its potential as a drug target and TSPO ligands have been shown to prevent neuronal loss in several animal models [13;67–69]. Broad-spectrum anti-inflammatory TSPO-binding ligands that penetrate the CNS readily may be useful in CNS inflammatory conditions. This investigation sheds light on the expression of TSPO in normal brain and in various

neuropathologic conditions, and may have a direct impact on understanding its potential as a pharmacological target and its uses in medical imaging.

Acknowledgments

The Manhattan HIV-1 Brain Bank of the National NeuroAIDS Tissue Consortium (NIH R24 MH59724) supplied much of the autopsy tissue. This study could not have been performed without the antibody from Dr. Pierre Casellas of Sanofi Synthelabo. The authors appreciate the generous sharing of tissues by Dr. Clayton Wiley (University of Pittsburg) and tissues and antibodies by Dr. Peter Davies (Albert Einstein College of Medicine). The authors acknowledge the input of Dr. Mary Rojas (Mount Sinai Adolescent Health Center), regarding the statistical analysis and Jacinta Murray (Mount Sinai Medical Center) for her assistance with ImageJ. The authors also greatly appreciate the support and encouragement of Dr. Cedric Raine throughout the course of this project. This study was supported by the City University of New York Research Foundation (PSC-CUNY 38-106 and 39-1059) and the NIH (RO1 MH55477 and the Einstein Center for AIDS Research P30 AI51519).

Abbreviations used

TSPO	Translocator protein of 18 kDa
CNS	central nervous system
PET	positron emission tomography
HIV	Human Immunodeficiency Virus-1
HIVE	Human Immunodeficiency Virus-1 Encephalitis
SIV	Simian Immunodeficiency Virus
SIVE	Simian Immunodeficiency Virus Encephalitis
AD	Alzheimer’s disease
PD	Parkinson’s disease
MS	multiple sclerosis
IHC	immunohistochemistry
TMA	tissue microarray
MGC	multinucleated giant cell
m.n	microglial nodules
pAb	polyclonal antibody
mAb	monoclonal antibody
w.m	white matter
g.m	gray matter
b.g	basal ganglia
N.A	not available
ht	hypertrophic
m.g	metabolic glia
DAB	diaminobenzidine
NNTC	National NeuroAIDS Tissue Consortium

References

1. Hanisch UK, Kettenmann H. Microglia: active sensor and versatile effector cells in the normal and pathologic brain. Nat Neurosci. 2007; 10:1387–1394. [PubMed: 17965659]
2. Glezer I, Simard AR, Rivest S. Neuroprotective role of the innate immune system by microglia. Neuroscience. 2007; 147:867–883. [PubMed: 17459594]
3. Garden GA, Moller T. Microglia biology in health and disease. J Neuroimmune Pharmacol. 2006; 1:127–137. [PubMed: 18040779]
4. Biber K, Neumann H, Inoue K, Boddeke HW. Neuronal 'On' and 'Off' signals control microglia. Trends Neurosci. 2007; 30:596–602. [PubMed: 17950926]
5. Lee, SC.; Cosenza, MA.; Si, Q.; Rivieccio, M.; Brosnan, CF. The CNS: Cells, Tissues, and Reactions to Insult. In: Ransohoff, RM.; Benveniste, EN., editors. Cytokines and the CNS. 2. Boca Raton, FL: Taylor & Francis Group; 2006. p. 1-22.
6. Rock RB, Peterson PK. Microglia as a pharmacological target in infectious and inflammatory diseases of the brain. J Neuroimmune Pharmacol. 2006; 1:117–126. [PubMed: 18040778]
7. Papadopoulos V. Peripheral-type benzodiazepine/diazepam binding inhibitor receptor: biological role in steroidogenic cell function. Endocr Rev. 1993; 14:222–240. [PubMed: 8391980]
8. Papadopoulos V, Amri H, Boujrad N, Cascio C, Culty M, Garnier M, Hardwick M, Li H, Vidic B, Brown AS, Reversa JL, Bernassau JM, Drieu K. Peripheral benzodiazepine receptor in cholesterol transport and steroidogenesis. Steroids. 1997; 62:21–28. [PubMed: 9029710]
9. Brown RC, Papadopoulos V. Role of the peripheral-type benzodiazepine receptor in adrenal and brain steroidogenesis. Int Rev Neurobiol. 2001; 46:117–143. [PubMed: 11599298]
10. Casellas P, Galiegue S, Basile AS. Peripheral benzodiazepine receptors and mitochondrial function. Neurochem Int. 2002; 40:475–486. [PubMed: 11850104]
11. Veenman L, Papadopoulos V, Gavish M. Channel-like functions of the 18-kDa translocator protein (TSPO): regulation of apoptosis and steroidogenesis as part of the host-defense response. Curr Pharm Des. 2007; 13:2385–2405. [PubMed: 17692008]
12. Choi HB, Khoo C, Ryu JK, van BE, Kim SU, McLarnon JG. Inhibition of lipopolysaccharide-induced cyclooxygenase-2, tumor necrosis factor-alpha and [Ca2+]i responses in human microglia by the peripheral benzodiazepine receptor ligand PK11195. J Neurochem. 2002; 83:546–555. [PubMed: 12390516]
13. Veiga S, Carrero P, Pernia O, Azcoitia I, Garcia-Segura LM. Translocator protein 18 kDa is involved in the regulation of reactive gliosis. Glia. 2007; 55:1426–1436. [PubMed: 17674368]
14. Venneti S, Lopresti BJ, Wiley CA. The peripheral benzodiazepine receptor (Translocator protein 18kDa) in microglia: from pathology to imaging. Prog Neurobiol. 2006; 80:308–322. [PubMed: 17156911]
15. Cagnin A, Kassiou M, Meikle SR, Banati RB. Positron emission tomography imaging of neuroinflammation. Neurotherapeutics. 2007; 4:443–452. [PubMed: 17599710]
16. James ML, Selleri S, Kassiou M. Development of ligands for the peripheral benzodiazepine receptor. Curr Med Chem. 2006; 13:1991–2001. [PubMed: 16842193]
17. Herholz K, Carter SF, Jones M. Positron emission tomography imaging in dementia. Br J Radiol. 2007; 80(Spec No 2):S160–S167. [PubMed: 18445746]
18. Chen MK, Guilarte TR. Translocator protein 18 kDa (TSPO): molecular sensor of brain injury and repair. Pharmacol Ther. 2008; 118:1–17. [PubMed: 18374421]
19. Hunakova L, Bodo J, Chovancova J, Sulikova G, Pastorekova S, Sedlak J. Expression of new prognostic markers, peripheral-type benzodiazepine receptor and carbonic anhydrase IX, in human breast and ovarian carcinoma cell lines. Neoplasma. 2007; 54:541–548. [PubMed: 17949239]
20. Maaser K, Grabowski P, Sutter AP, Hopfner M, Foss HD, Stein H, Berger G, Gavish M, Zeitz M, Scherubl H. Overexpression of the peripheral benzodiazepine receptor is a relevant prognostic factor in stage III colorectal cancer. Clin Cancer Res. 2002; 8:3205–3209. [PubMed: 12374690]
21. Galiegue S, Casellas P, Kramar A, Tinel N, Simony-Lafontaine J. Immunohistochemical assessment of the peripheral benzodiazepine receptor in breast cancer and its relationship with survival. Clin Cancer Res. 2004; 10:2058–2064. [PubMed: 15041726]

22. Ryu JK, Choi HB, McLarnon JG. Peripheral benzodiazepine receptor ligand PK11195 reduces microglial activation and neuronal death in quinolinic acid-injected rat striatum. Neurobiol Dis. 2005; 20:550–561. [PubMed: 15916899]

23. Cosenza MA, Zhao ML, Si Q, Lee SC. Human brain parenchymal microglia express CD14 and CD45 and are productively infected by HIV-1 in HIV-1 encephalitis. Brain Pathol. 2002; 12:442–455. [PubMed: 12408230]

24. Cosenza-Nashat M, Zhao ML, Marshall HD, Si Q, Morgello S, Lee SC. Human immunodeficiency virus infection inhibits granulocyte-macrophage colony-stimulating factor-induced microglial proliferation. J Neurovirol. 2007; 13:536–548. [PubMed: 18097885]

25. Bissel SJ, Wang G, Bonneh-Barkay D, Starkey A, Trichel AM, Murphey-Corb M, Wiley CA. Systemic and brain macrophage infections in relation to the development of simian immunodeficiency virus encephalitis. J Virol. 2008; 82:5031–5042. [PubMed: 18337567]

26. Cosenza MA, Zhao ML, Shankar SL, Shafit-Zagardo B, Lee SC. Up-regulation of MAP2e-expressing oligodendrocytes in the white matter of patients with HIV-1 encephalitis. Neuropathol Appl Neurobiol. 2002; 28:480–488. [PubMed: 12445164]

27. Morgan J, Oseroff AR, Cheney RT. Expression of the peripheral benzodiazepine receptor is decreased in skin cancers in comparison with normal skin. Br J Dermatol. 2004; 151:846–856. [PubMed: 15491426]

28. Bribes E, Carriere D, Goubet C, Galiegue S, Casellas P, Simony-Lafontaine J. Immunohistochemical assessment of the peripheral benzodiazepine receptor in human tissues. J Histochem Cytochem. 2004; 52:19–28. [PubMed: 14688214]

29. Abramoff MC, Magelhaes PJ, Ram SJ. Image Processing with ImageJ. Biophotonics International. 2004; 11:36–42.

30. Rangan GK, Tesch GH. Quantification of renal pathology by image analysis. Nephrology (Carlton). 2007; 12:553–558. [PubMed: 17995580]

31. Tomasi G, Edison P, Bertoldo A, Roncaroli F, Singh P, Gerhard A, Cobelli C, Brooks DJ, Turkheimer FE. Novel reference region model reveals increased microglial and reduced vascular binding of 11C-(R)-PK11195 in patients with Alzheimer's disease. J Nucl Med. 2008; 49:1249–1256. [PubMed: 18632810]

32. Cosenza-Nashat MA, Kim MO, Zhao ML, Suh HS, Lee SC. CD45 isoform expression in microglia and inflammatory cells in HIV-1 encephalitis. Brain Pathol. 2006; 16:256–265. [PubMed: 17107594]

33. Kuhlmann AC, Guilarte TR. Cellular and subcellular localization of peripheral benzodiazepine receptors after trimethyltin neurotoxicity. J Neurochem. 2000; 74:1694–1704. [PubMed: 10737628]

34. Benavides J, Dubois A, Gotti B, Bourdiol F, Scatton B. Cellular distribution of omega 3 (peripheral type benzodiazepine) binding sites in the normal and ischaemic rat brain: an autoradiographic study with the photoaffinity ligand [3H]PK 14105. Neurosci Lett. 1990; 114:32–38. [PubMed: 2166260]

35. Weissman BA, Bolger GT, Isaac L, Paul SM, Skolnick P. Characterization of the binding of [3H]Ro 5–4864, a convulsant benzodiazepine, to guinea pig brain. J Neurochem. 1984; 42:969–975. [PubMed: 6321666]

36. Karchewski LA, Bloechlinger S, Woolf CJ. Axonal injury-dependent induction of the peripheral benzodiazepine receptor in small-diameter adult rat primary sensory neurons. Eur J Neurosci. 2004; 20:671–683. [PubMed: 15255978]

37. Mankowski JL, Queen SE, Tarwater PJ, Adams RJ, Guilarte TR. Elevated peripheral benzodiazepine receptor expression in simian immunodeficiency virus encephalitis. J Neurovirol. 2003; 9:94–100. [PubMed: 12587072]

38. Stoebner PE, Carayon P, Penarier G, Frechin N, Barneon G, Casellas P, Cano JP, Meynadier J, Meunier L. The expression of peripheral benzodiazepine receptors in human skin: the relationship with epidermal cell differentiation. Br J Dermatol. 1999; 140:1010–1016. [PubMed: 10354064]

39. Takaya S, Hashikawa K, Turkheimer FE, Mottram N, Deprez M, Ishizu K, Kawashima H, Akiyama H, Fukuyama H, Banati RB, Roncaroli F. The lack of expression of the peripheral

benzodiazepine receptor characterises microglial response in anaplastic astrocytomas. J Neurooncol. 2007; 85:95–103. [PubMed: 17520179]

40. Maaser K, Grabowski P, Oezdem Y, Krahn A, Heine B, Stein H, Buhr H, Zeitz M, Scherubl H. Up-regulation of the peripheral benzodiazepine receptor during human colorectal carcinogenesis and tumor spread. Clin Cancer Res. 2005; 11:1751–1756. [PubMed: 15755996]
41. Banati RB. Visualising microglial activation in vivo. Glia. 2002; 40:206–217. [PubMed: 12379908]
42. Vlodavsky E, Soustiel JF. Immunohistochemical expression of peripheral benzodiazepine receptors in human astrocytomas and its correlation with grade of malignancy, proliferation, apoptosis and survival. J Neurooncol. 2007; 81:1–7. [PubMed: 16868661]
43. Miettinen H, Kononen J, Haapasalo H, Helen P, Sallinen P, Harjuntausta T, Helin H, Alho H. Expression of peripheral-type benzodiazepine receptor and diazepam binding inhibitor in human astrocytomas: relationship to cell proliferation. Cancer Res. 1995; 55:2691–2695. [PubMed: 7780986]
44. Venneti S, Lopresti BJ, Wang G, Hamilton RL, Mathis CA, Klunk WE, Apte UM, Wiley CA. PK11195 labels activated microglia in Alzheimer's disease and in vivo in a mouse model using PET. Neurobiol Aging. 2008
45. Banati RB, Goerres GW, Myers R, Gunn RN, Turkheimer FE, Kreutzberg GW, Brooks DJ, Jones T, Duncan JS. [11C](R)-PK11195 positron emission tomography imaging of activated microglia in vivo in Rasmussen's encephalitis. Neurology. 1999; 53:2199–2203. [PubMed: 10599809]
46. Maeda J, Higuchi M, Inaji M, Ji B, Haneda E, Okauchi T, Zhang MR, Suzuki K, Suhara T. Phase-dependent roles of reactive microglia and astrocytes in nervous system injury as delineated by imaging of peripheral benzodiazepine receptor. Brain Res. 2007; 1157:100–111. [PubMed: 17540348]
47. Chen MK, Guilarte TR. Imaging the peripheral benzodiazepine receptor response in central nervous system demyelination and remyelination. Toxicol Sci. 2006; 91:532–539. [PubMed: 16554315]
48. Lavoie J, Layrargues GP, Butterworth RF. Increased densities of peripheral-type benzodiazepine receptors in brain autopsy samples from cirrhotic patients with hepatic encephalopathy. Hepatology. 1990; 11:874–878. [PubMed: 2161396]
49. Alho H, Varga V, Krueger KE. Expression of mitochondrial benzodiazepine receptor and its putative endogenous ligand diazepam binding inhibitor in cultured primary astrocytes and C-6 cells: relation to cell growth. Cell Growth Differ. 1994; 5:1005–1014. [PubMed: 7819126]
50. Venneti S, Lopresti BJ, Wang G, Bissel SJ, Mathis CA, Meltzer CC, Boada F, Capuano S III, Kress GJ, Davis DK, Ruszkiewicz J, Reynolds IJ, Murphey-Corb M, Trichel AM, Wisniewski SR, Wiley CA. PET imaging of brain macrophages using the peripheral benzodiazepine receptor in a macaque model of neuroAIDS. J Clin Invest. 2004; 113:981–989. [PubMed: 15057304]
51. Wiley CA, Lopresti BJ, Becker JT, Boada F, Lopez OL, Mellors J, Meltzer CC, Wisniewski SR, Mathis CA. Positron emission tomography imaging of peripheral benzodiazepine receptor binding in human immunodeficiency virus-infected subjects with and without cognitive impairment. J Neurovirol. 2006; 12:262–271. [PubMed: 16966217]
52. Venneti S, Bonneh-Barkay D, Lopresti BJ, Bissel SJ, Wang G, Mathis CA, Piatak M Jr, Lifson JD, Nyaundi JO, Murphey-Corb M, Wiley CA. Longitudinal in vivo positron emission tomography imaging of infected and activated brain macrophages in a macaque model of human immunodeficiency virus encephalitis correlates with central and peripheral markers of encephalitis and areas of synaptic degeneration. Am J Pathol. 2008; 172:1603–1616. [PubMed: 18467697]
53. Venneti S, Wang G, Wiley CA. The high affinity peripheral benzodiazepine receptor ligand DAA1106 binds to activated and infected brain macrophages in areas of synaptic degeneration: implications for PET imaging of neuroinflammation in lentiviral encephalitis. Neurobiol Dis. 2008; 29:232–241. [PubMed: 17920902]
54. Dussossoy D, Carayon P, Feraut D, Belugou S, Combes T, Canat X, Vidal H, Casellas P. Development of a monoclonal antibody to immuno-cytochemical analysis of the cellular localization of the peripheral benzodiazepine receptor. Cytometry. 1996; 24:39–48. [PubMed: 8723901]

55. Mills C, Makwana M, Wallace A, Benn S, Schmidt H, Tegeder I, Costigan M, Brown RH Jr, Raivich G, Woolf CJ. Ro5–4864 promotes neonatal motor neuron survival and nerve regeneration in adult rats. Eur J Neurosci. 2008; 27:937–946. [PubMed: 18333964]
56. Zhang K, Demeure O, Belliard A, Goujon JM, Favreau F, Desurmont T, Mauco G, Barriere M, Carretier M, Milan D, Papadopoulos V, Hauet T. Cloning, sequencing, and chromosomal localization of pig peripheral benzodiazepine receptor: three different forms produced by alternative splicing. Mamm Genome. 2006; 17:1050–1062. [PubMed: 17019653]
57. Lin D, Chang YJ, Strauss JF III, Miller WL. The human peripheral benzodiazepine receptor gene: cloning and characterization of alternative splicing in normal tissues and in a patient with congenital lipoid adrenal hyperplasia. Genomics. 1993; 18:643–650. [PubMed: 8307574]
58. Costa B, Salvetti A, Rossi L, Spinetti F, Lena A, Chelli B, Rechichi M, Da PE, Gremigni V, Martini C. Peripheral benzodiazepine receptor: characterization in human T-lymphoma Jurkat cells. Mol Pharmacol. 2006; 69:37–44. [PubMed: 16189298]
59. Fujita M, Imaizumi M, Zoghbi SS, Fujimura Y, Farris AG, Suhara T, Hong J, Pike VW, Innis RB. Kinetic analysis in healthy humans of a novel positron emission tomography radioligand to image the peripheral benzodiazepine receptor, a potential biomarker for inflammation. Neuroimage. 2008; 40:43–52. [PubMed: 18093844]
60. Petit-Taboue MC, Baron JC, Barre L, Travere JM, Speckel D, Camsonne R, MacKenzie ET. Brain kinetics and specific binding of [11C]PK 11195 to omega 3 sites in baboons: positron emission tomography study. Eur J Pharmacol. 1991; 200:347–351. [PubMed: 1782994]
61. Giatzakis C, Batarseh A, Dettin L, Papadopoulos V. The role of Ets transcription factors in the basal transcription of the translocator protein (18 kDa). Biochemistry. 2007; 46:4763–4774. [PubMed: 17402746]
62. Rey C, Mauduit C, Naureils O, Benahmed M, Louisot P, Gasnier F. Up-regulation of mitochondrial peripheral benzodiazepine receptor expression by tumor necrosis factor alpha in testicular leydig cells. Possible involvement in cell survival. Biochem Pharmacol. 2000; 60:1639–1646. [PubMed: 11077046]
63. Bourdiol F, Toulmond S, Serrano A, Benavides J, Scatton B. Increase in omega 3 (peripheral type benzodiazepine) binding sites in the rat cortex and striatum after local injection of interleukin-1, tumour necrosis factor-alpha and lipopolysaccharide. Brain Res. 1991; 543:194–200. [PubMed: 1647831]
64. Oh YJ, Francis JW, Markelonis GJ, Oh TH. Interleukin-1-beta and tumor necrosis factor-alpha increase peripheral-type benzodiazepine binding sites in cultured polygonal astrocytes. J Neurochem. 1992; 58:2131–2138. [PubMed: 1573395]
65. Trincavelli ML, Marselli L, Falleni A, Gremigni V, Ragge E, Dotta F, Santangelo C, Marchetti P, Lucacchini A, Martini C. Upregulation of mitochondrial peripheral benzodiazepine receptor expression by cytokine-induced damage of human pancreatic islets. J Cell Biochem. 2002; 84:636–644. [PubMed: 11813268]
66. Papadopoulos V, Lecanu L, Brown RC, Han Z, Yao ZX. Peripheral-type benzodiazepine receptor in neurosteroid biosynthesis, neuropathology and neurological disorders. Neuroscience. 2006; 138:749–756. [PubMed: 16338086]
67. Schwartz-Bloom RD, Miller KA, Evenson DA, Crain BJ, Nadler JV. Benzodiazepines protect hippocampal neurons from degeneration after transient cerebral ischemia: an ultrastructural study. Neuroscience. 2000; 98:471–484. [PubMed: 10869841]
68. Veiga S, Azcoitia I, Garcia-Segura LM. Ro5–4864, a peripheral benzodiazepine receptor ligand, reduces reactive gliosis and protects hippocampal hilar neurons from kainic acid excitotoxicity. J Neurosci Res. 2005; 80:129–137. [PubMed: 15696538]
69. Soustiel JF, Zaaroor M, Vlodavsky E, Veenman L, Weizman A, Gavish M. Neuroprotective effect of Ro5–4864 following brain injury. Exp Neurol. 2008
70. Morgello S, Gelman BB, Kozlowski PB, Vinters HV, Masliah E, Cornford M, Cavert W, Marra C, Grant I, Singer EJ. The National NeuroAIDS Tissue Consortium: a new paradigm in brain banking with an emphasis on infectious disease. Neuropathol Appl Neurobiol. 2001; 27:326–335. [PubMed: 11532163]

71. Desruisseaux MS, Gulinello M, Smith DN, Lee SC, Tsuji M, Weiss LM, Spray DC, Tanowitz HB. Cognitive dysfunction in mice infected with Plasmodium berghei strain ANKA. J Infect Dis. 2008; 197:1621–1627. [PubMed: 18419550]

72. Mankowski JL, Carter DL, Spelman JP, Nealen ML, Maughan KR, Kirstein LM, Didier PJ, Adams RJ, Murphey-Corb M, Zink MC. Pathogenesis of simian immunodeficiency virus pneumonia: an immunopathological response to virus. Am J Pathol. 1998; 153:1123–1130. [PubMed: 9777943]

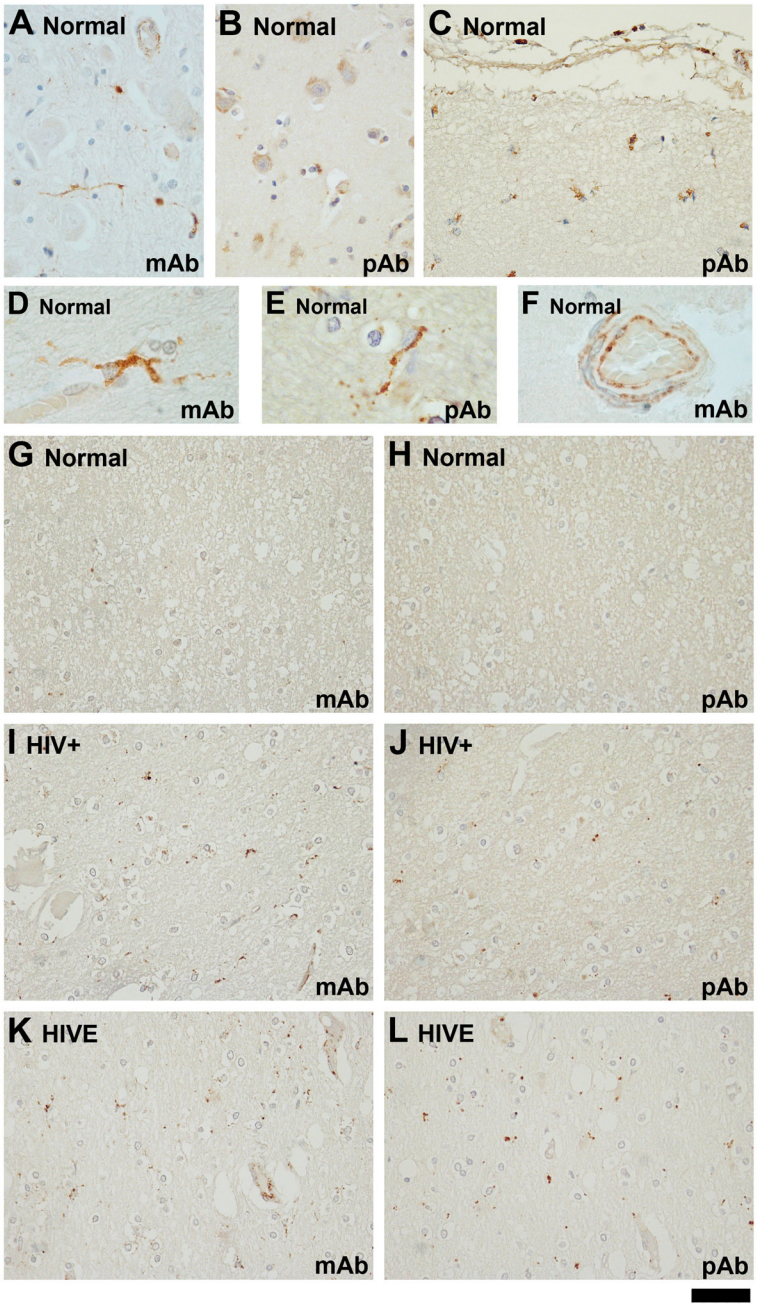

Figure 1. Comparison of monoclonal (mAb) and polyclonal (pAb) anti-TSPO antibodies in human CNS

Staining is present in both grey matter (A, B) and white matter (G, H) glial cells of normal human brain. The pAb has some staining of neurons (B), which is not observed with the mAb (A). The staining in normal brain is minimal, in general, although there is some case variation (see Figure 3, Table 3) and subpial glia (C) and ependymal cells (not shown) routinely express the TSPO. Under high power, most positively stained parenchymal cells have microglial morphology (D, E). Endothelial cell staining is more often observed with the mAb than with the pAb (F). Despite these differences, the two antibodies have good agreement with their staining in the white matter. The same normal case (G, H), HIV-

seropositive case (I, J) and HIVE case (K, L) are stained with both antibodies as indicated. The scale bar represents 50 μm for A–C and G–L, but 20 μm in D–F.

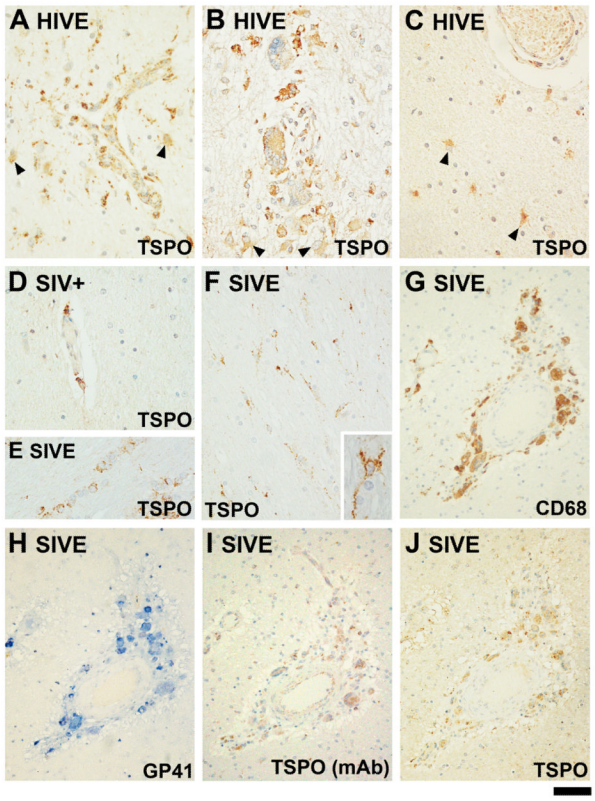

Figure 2. Expression of TSPO in HIVE and in the SIV model in macaques

TSPO is shown in three cases of HIVE (A–C). The staining is with the pAb unless indicated otherwise. The microglial nodule shown in A is laden with TSPO+ perivascular cells and TSPO+ astrocytes are present. In all panels, TSPO+ astrocytes are indicated with arrowheads and cells were identified based on morphology. The microglial nodule shown in B is full of TSPO+ multinucleated giant cells. The area shown in (C), away from a microglial nodule, shows TSPO+ astrocytes adjacent to a vessel. (D) Perivascular TSPO+ cells are shown in an SIV+ brain without encephalitis. TSPO+ perivascular cells are also present in SIV− brain (not shown). (E) illustrates TSPO+ oligodendrocytes, based on the typical linear arrangement. (F) displays ramified microglia (based on morphology) observed throughout the parenchyma in one SIVE brain. One TSPO+ cell is shown in high power in the inset of (F). (G–J) are serial sections of the same microglial nodule stained for CD68: (G), SIV GP41 (H), the TSPO mAb (I) and the TSPO pAb (J). The scale bar represents 40 μm in A–F, 80μm in G–J and 12 μm in F inset.

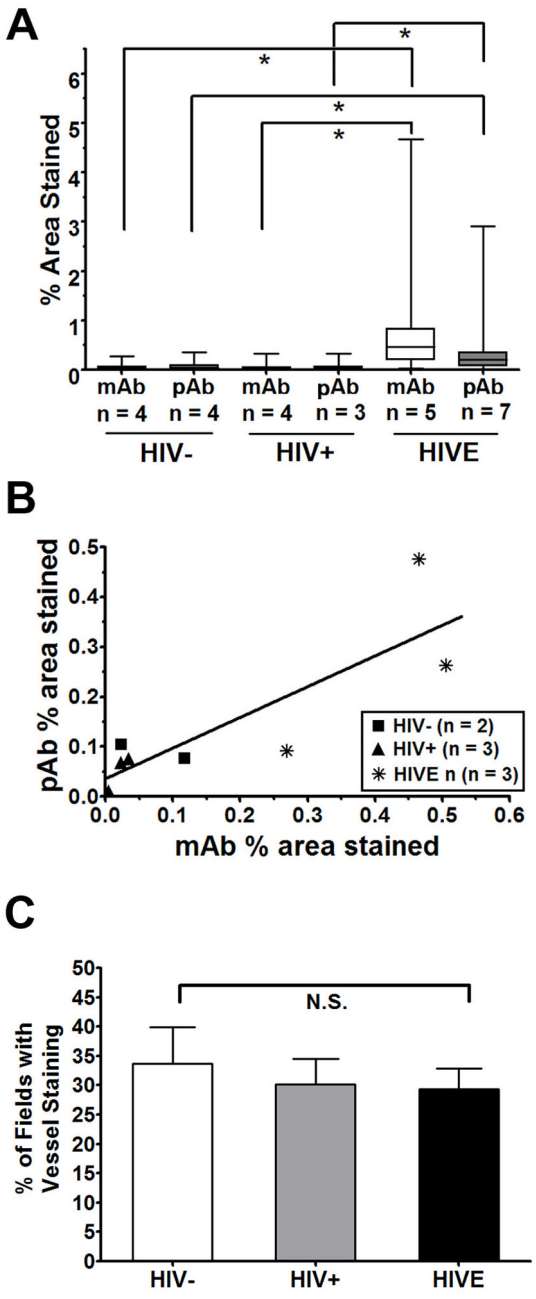

Figure 3. Image analysis of TSPO immunohistochemistry for HIVE and controls

Image analysis of TSPO was completed for twenty 400X microscope fields of white matter per case for each antibody. (A) Staining is expressed as the percent area stained as analyzed with NIH ImageJ, as described in the Methods. The data are represented as the median ± range with the box indicating the 25th and 75th quartiles. The average percent area stained for sections immunolabeled with the monoclonal antibody (mAb, white boxes) and sections labeled with the polyclonal antibody (pAb, grey boxes) are shown. Asterisks denote p <0.001 by Kruskal-Wallis analysis of variance followed by Dunn's multiple comparison test. (B) For cases where serial sections from the same case were available for both the mAb and the pAb (total n = 8), a Spearman correlation analysis was performed which indicated a

significant correlation ($p < 0.05$; $r = 0.83$). (C) Sections stained with the mAb were analyzed for vessel staining as described in the Methods. The percent of fields where vessel staining was evident was not significantly different between HIV−, HIV+ and HIVE based on one-way analysis of variance ($p > 0.05$). N.S. = not significant.

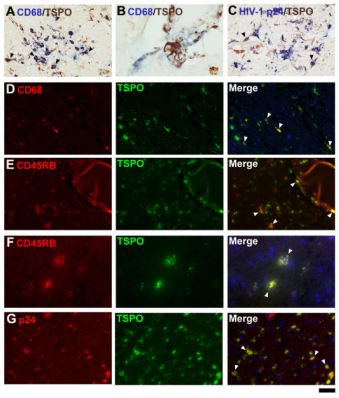

Figure 4. Double-immunohistochemistry for TSPO and microglial markers in HIVE

In HIVE, the majority of TSPO-expressing cells are microglia, as shown with CD68 labeling (A, B, D panels) and CD45RB (E and F panels). Multinucleated giant cells are double labeled (B). HIV-infected cells express TSPO as seen in microglial nodules stained for HIV-1 p24 (C, G panels). Arrowheads illustrate some cells double-labeled for both markers. The scale bar represent 30 μm in A, C and 12μm in B, 50 μm in D, E and G and 25 μm in F.

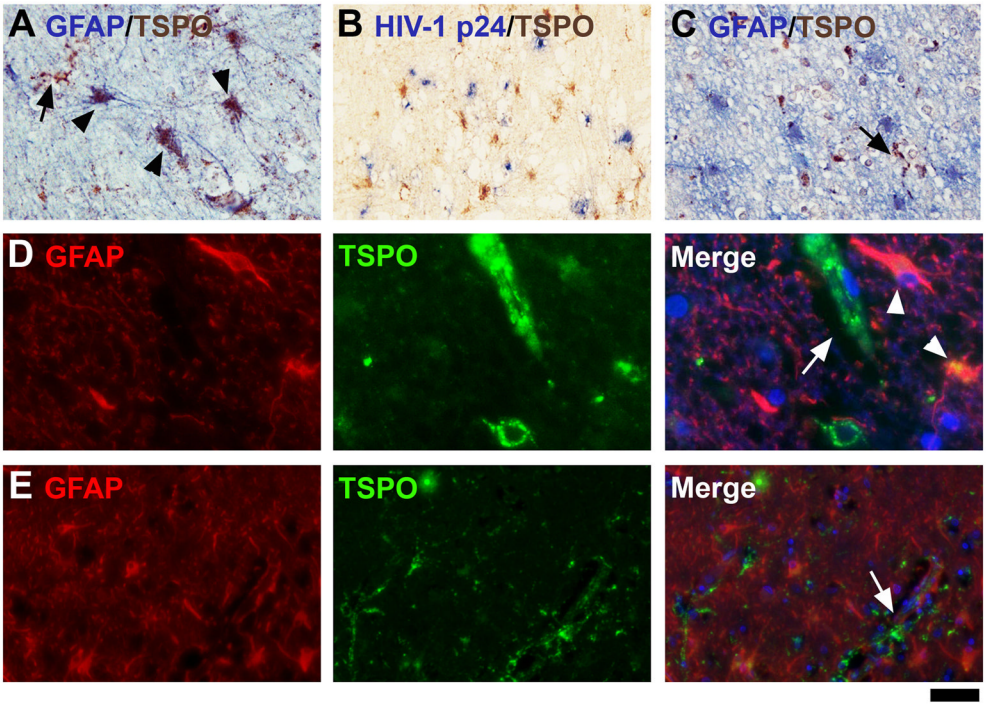

Figure 5. TSPO in astrocytes in HIVE

All cases of HIVE displayed some degree of astrocytic expression. One case with relatively high astrocytic expression of the TSPO is shown with double-label IHC for GFAP (A, D panels). The same case is stained for TSPO with HIV-1 p24 (B). Two other cases with less astrocytic staining are shown (C, E panels). Note that GFAP+ astrocytes are not double-labeled in these cases. Double-labeled astrocytes are indicated with arrowheads, while TSPO-expressing microglia ($GFAP^{-}$) are indicated with arrows. The scale bar represents 30 μm in A and C, 60 μm in B, 12.5 μm in D and 50 μm in E.

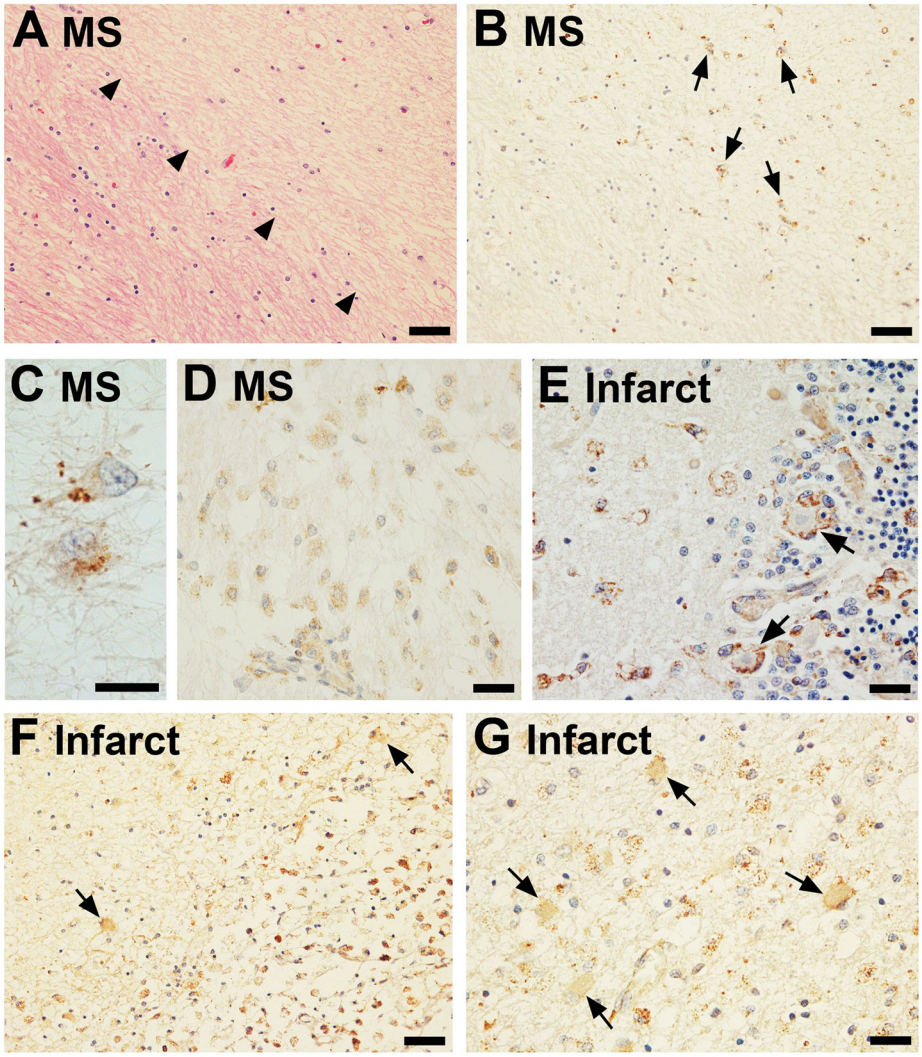

Figure 6. TSPO expression in multiple sclerosis (MS) and ischemic stroke

An area of demyelination is demarcated by arrowheads in an MS brain (H&E, A) and the same region of this plaque shows high TSPO labeling in the demyelinated area (arrows, B) as imaged from a serial section of the same block. TSPO+ cells in the old plaque are most likely fibrillary astrocytes (shown in high power in C). In an active plaque, TSPO+ amoeboid macrophages are prominent (D). Transforming microglia around Purkinje cells display strong TSPO positivity and are observed in a sub-acute infarct (E). TSPO+ cells can be observed juxtaposed to the neurons (arrows, E). Bordering a chronic infarct were TSPO+ cells with astrocytic morphology (arrows, F, G), as well as amoeboid cells. The scale bars represent 50 μm in A, B and F; 25 μm in D,E and G; and 15 μm in C.

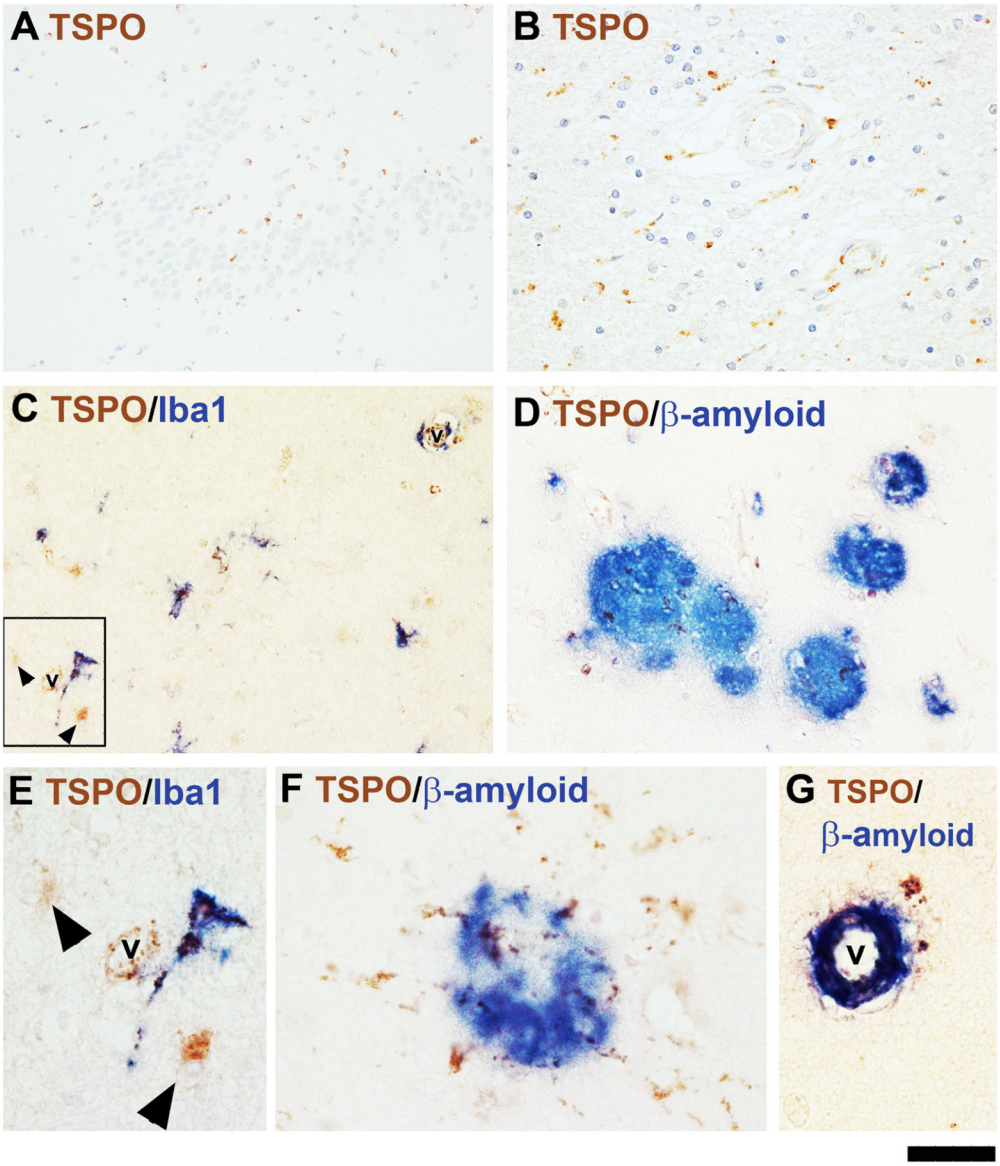

Figure 7. TSPO expression in Alzheimer's disease (AD)

TSPO is present in glial cells sprinkled throughout the dentate gyrus and the adjacent areas (A) as well as in the hippocampal white matter (B). Glial cells expressing TSPO included Iba1+ microglial cells (C, E) as well as Iba1-negative cells, with astroglial morphology (arrows, C, E). The region in E is a high power image of the boxed region in (C). Note the dark spots within the cytoplasm (TSPO stain) of the Iba1+ ramified cell and the swollen nuclei of the astrocyte-like cells in E. TSPO+ cells were also found associating with senile plaques. Aβ+ plaques of various sizes are shown in (D) and TSPO+ glial cells radiate from one plaque (F, high power). A vessel with amyloid angiopathy was also TSPO+ (G). The scale bar represents 100 μm in A; 50 μm in B, C and D; and 20 μm in E, F and G. v = vessel lumen.

Table 1

Sources of tissue samples

Disease Status	Tissue Source (Reference)	Number of specimens	Brain Regions Studied
Normal (HIV−), HIV+ and HIVE	National NeuroAIDS Tissue Consortium, Manhattan HIV-1 Brain Bank [70]	4, 5 and10	Cerebral cortex and associated white matter in most
SIV−, SIV+ and SIVE	University of Pittsburgh Graduate School of Public Health, courtesy of Dr. Clayton Wiley	1, 1 and 2	Anterior basal ganglia with associated cerebral cortex and white matter
Alzheimer's disease	Albert Einstein College of Medicine, courtesy of Dr. Peter Davies	9	Hippocampus
Ischaemic infarct	Albert Einstein College of Medicine, Division of Neuropathology Archives	3	Basal ganglia, cerebellum, cerebral cortex with associated white matter
Multiple sclerosis	Albert Einstein College of Medicine Division of Neuropathology Archives (n = 2), National NeuroAIDS Tissue Consortium, Manhattan HIV-1 Brain Bank (n = 1) [70]	3	Periventricular white matter, pons, cerebellum

Neuropathol Appl Neurobiol. Author manuscript; available in PMC 2009 June 8.

Table 2

Antibody sources and methods

Antigen (antibody type)	Primary Antibody Source	Dilution Used	Colorimetric Immunohistochemical Method	Fluorescent Immunohistochemical Method*	Method Reference for Colorimetric IHC
TSPO (polyclonal)	Janet Morgan (Roswell Park Cancer Institute)	1:500	Avidin-Biotin Complex Method LSAB2 kit (DAKO) with hematoxylin counterstain	Avidin Kit (Vector Laboratories, Ltd., Burlingame, CA) with fluorescein-conjugated streptavidin with DAPI counterstain	[27]
TSPO (monoclonal, 8D7)	Pierre Casellas (Sanofi Synthelabo)	1:350	ImmPRESS anti-mouse peroxidase kit (Vector Laboratories, Ltd.) with hematoxylin counterstain	Avidin Kit (Vector Laboratories, Ltd.) with fluorescein-conjugated streptavidin with DAPI counterstain	[28] Staining methods were modified for this study.
GFAP (polyclonal)	Biogenex (San Ramon, CA)	1:250	Primary with goat anti-rabbit alkaline phosphatase-conjugated secondary	Primary with goat anti-rabbit Alexa fluorophor 594-conjugated secondary antibody with DAPI counterstain	[26]
CD45RB (monoclonal, clone MT4)	Pharmingen	1:100	Not performed for this study	Primary with goat anti-mouse Alexa fluorophor 594-conjugated secondary antibody with DAPI counterstain	[32]
CD68 (monoclonal, clone KP1)	DAKO (Carpinteria, CA)	1:600	Primary with goat anti-rabbit alkaline phosphatase-conjugated secondary	Primary with goat anti-mouse Alexa fluorophor 594-conjugated secondary antibody with DAPI counterstain	[23]
Iba1 (polyclonal)	Wako Pure Chemical Industries, Ltd. (Richmond, VA)	1:500	Avidin-Biotin Complex Method with Vectastain kit, Alkaline Phosphatase (Vector Laboratories, Ltd.)	Not performed for this study	[71]
HIV-1 p24 (monoclonal, clone MIB-1)	DAKO	1:10	Primary with goat anti-rabbit alkaline phosphatase-conjugated secondary	Primary with goat anti-mouse Alexa fluorophor 594-conjugated secondary antibody with DAPI counterstain	[23]
SIV mac251 gp41 (monoclonal, clone KK41)	NIH AIDS Research and Reference Reagent Program (Dr. Karen Kent and Miss Caroline Powell)	1:200	Avidin-Biotin Complex Method with Vectastain kit, Peroxidase (Vector Laboratories, Ltd.) with hematoxylin counterstain	Not performed for this study	[72]
β-amyloid 40 (monoclonal, clone 11A5)	Peter Davies (Albert Einstein College of Medicine)	1:1000	Avidin-Biotin Complex Method with Vectastain kit, Peroxidase (Vector Laboratories, Ltd.)	Not performed for this study	P. Davies, personal communication

*Fluorescent methods were devised for the current study.

Table 3

Summary of TSPO immunoreactivity in HIVE/SIVE and control cases

HIV/SIV status	Case	Brain region studied	[1] Notable pathology	Antibody	[3] Microglia/Macrophages	[3] Astrocytes	[3] Neurons	[3] Vessel Stain
HIV−	16	White matter ([2] w.m.)		[2] p	++	+	+	+
				[2] m	++	±	-	+
	18	Cortex and w.m.		p	+	+	+	+
				m	+	±	−	+
	19	Cortex and w.m.		p	+	−	+	+
				m	+	+	−	+
	28	Cortex and w.m.		p	±	−	−	-
				m	+	−	−	+
HIV+	13	Cortex and w.m.		p	+	+ metabolic glia ([2] m.g.)	+	+
				m	+	+ m.g.	−	+
	14	Cortex and w.m.		[2] N.A.				
				m	±	−	−	+
	15	Cortex and w.m.		p	++	+ m.g.	+	+
				m	++	+ m.g.	−	+
	25	Cortex and w.m.		p	−	−	±	±
				m	−	−	−	+
	26	Cortex and w.m.		p	−	−	±	±
				m		−	−	+
HIVE	1	Cortex and w.m.		p	+++	+	±	+
				N.A.				
	[4]3	[5] Gray matter ([2] g.m.)/w.m.	Diffuse HIV, prominent multinucleated giant cells ([2] m.g.c.)	p	++++	++ hyper-trophic ([2] ht)	+	+
				N.A.				
	4	G.m./w.m.		p	++	++ ht	++	+
				m	++	++ ht	−	++
	5	W.m.		p	+	+	N.A.	+

HIV/SIV status	Case	Brain region studied	[1] Notable pathology	Antibody	[3] Microglia/Macrophages	[3] Astrocytes	[3] Neurons	[3] Vessel Stain
				N.A.				
	8	Basal ganglia ([2] b.g.)	Prominent microglial nodules ([2] m.n.)	p	+++	++ ht	++	+
				m	+++	++ ht		++
	9	Cortex and w.m.		p	++	+ ht	++	+
				m	++	++ ht		+
	20	Cortex and w.m.		p	++	+ ht	+	+
				N.A.				
	22	W.m.	Macrophages/amoeboid microglia	p	+	++ ht	N.A.	+
				m	++	+ ht	N.A.	++
	[4]23	Multiple areas (Cortex and w.m.)	Prominent m.n., lymphoma	p	+++	++ ht	++	+
				m	+++	+ ht		++
	38	Cortex and w.m.	Diffuse vacuoles	p	++++	++ ht	+	+
				m	+++	+ ht		+
SIV−	CW97–421	Anterior b.g. & adjacent cortex and w.m.		p	−	−	+	±
				m	−	−	−	+
SIV+	CW99–224	Anterior b.g. & adjacent cortex and w.m.		p	±	−	±	+
				m	−	−	−	+
SIVE	CW00–221	Anterior b.g. & adjacent cortex and w.m.	prominent m.g.c.	p	++	−	+	±
			and focal gliosis	m	+++	−	−	+
	CW00–220	Anterior b.g. & adjacent cortex and w.m.	Diffuse microgliosis	p	+++	−	+	+
				m	++++	−	−	++

[1]For HIVE and SIVE, standard pathology, including multinucleated giant cells and microglial nodules, was present. Notable pathology is in addition to standard pathology.

[2]Abbreviations used: white matter (w.m.), polyclonal (p), monoclonal (m), gray matter (g.m.), basal ganglia (b.g.), multinucleated giant cells (m.g.c.), microglial nodules (m.n.), not available (N.A.), hypertrophic (h.t.) and metabolic glia (m.g.).

[3]The semi-quantitative grading system was applied to the average number of cells in ten 400X fields such that (−) indicates no staining; (±), TSPO+ punctuate spots only; (+), 1–5 TSPO+ cells; (++), 5–10 TSPO+ cells; (+++), 10–15 TSPO+ cells and (++++), 15 –>20 TSPO+ cells. TSPO+ Neurons were only assessed when gray matter was present. Astrocytes may be hypertrophic (ht) or metabolic glia (m.g.). Vessel staining includes both TSPO+ endothelial cells and smooth muscle cells.

[4] Case 23 is the lymphoma case; Case 3 also had neurosyphillis.

[5] The term "gray matter" is used when the anatomic region cannot be positively identified from the section.